Springer

Journal of
Mechanical
Science and
Technology

Journal of Mechanical Science and Technology 22 (2008) 1417~1425

www.springerlink.com/content/1738-494x

Numerical analysis on the performance of cooling plates in a PEFC

Jongmin Choi[1], Yoon-Ho Kim[2], Yongtaek Lee[2], Kyu-Jung Lee[3] and Yongchan Kim[3,*]

[1]*Department of Mechanical Engineering, Hanbat National University, Duckmyung-Dong, Yusung-Gu, Daejeon, 305-719, KOREA*
[2]*Graduate School of Mechanical Engineering, Korea University, Anam-Dong, Sungbuk-Gu, Seoul, 136-701, KOREA*
[3]*Department of Mechanical Engineering, Korea University, Anam-Dong, Sungbuk-Gu, Seoul, 136-701, KOREA*

(Manuscript Received January 18, 2008; Revised March 10, 2008; Accepted April 14, 2008)

Abstract

Among the various types of fuel cells, the polymer electrolyte fuel cell (PEFC) is one of the prospective power sources for automotive applications, stationary cogeneration systems, and mobile electronic devices. The PEFC is very sensitive to the high temperature environment inside the fuel cell, and non-uniform temperature distribution reduces its performance. In this study, the performance of cooling plates for the PEFC was investigated by using three-dimensional computational fluid dynamics with commercial software. Six cooling plates were designed with different channel configurations. Models 1 and 4 had typical serpentine and parallel configurations, respectively. Models 2 and 3 had modified serpentine structures from Model 1, while Models 5 and 6 had modified parallel structures from Model 4. Models 1 and 2 showed relatively high temperatures around the outlet and the inlet area of the channel, respectively. Cooling performance of Models 4 and 5 was lower than that of Model 6 due to non-uniform fluid flow and temperature distributions. Models 3 and 6 showed higher cooling performance than serpentine type models and parallel type models, respectively. The performance of Model 3 was superior to that of Model 6 with respect to the control of the maximum surface temperature and uniformity. The thermal performance of Model 3 improved over Model 6 with the increase of heat flux. However, the pressure drop of Model 3 was higher than that of Model 6 because Model 3 had relatively high flow velocity through its channel and greater number of bends than Model 6.

Keywords: Polymer electrolyte fuel cell; Thermal reliability; Pressure drop; Cooling plate

1. Introduction

A fuel cell is an electrochemical energy device that converts chemical energy in the fuel directly into electrical energy. Therefore, the fuel cell represents higher efficiency and better environmental compatibility over conventional power supply devices. It is considered a promising viable direct energy conversion technology [1-3].

Among the various types of fuel cells, the polymer electrolyte fuel cell (PEFC) is one of the prospective power sources in automotive applications, stationary cogeneration systems, and mobile electronic devices. The PEFC shows higher power density and faster start-up than other fuel cells. In addition, it offers design simplicity and works in the moderate range of cell operating temperatures [4].

Inside a PEFC stack, an electrochemical reaction between hydrogen and oxygen occurs through membrane electrode assembly (MEA), and it produces electricity, water, and heat. PEFCs are very sensitive to high temperature conditions inside a fuel cell, and the non-uniform temperature distribution inside a fuel cell degrades the performance of a PEFC. Therefore, a properly designed cooling system of a fuel cell for the PEFC is very essential to improve the performance and reliability of the PEFC [5, 6].

The heat and mass transfer mechanism has been investigated for the reactant studies in the PEFC. Nguyen and White [7] studied the variation in current density, water transport, and flow temperatures along

*Corresponding author. Tel.: +82 2 3290 3366, Fax.: +82 2 921 5439
E-mail address: yongckim@korea.ac.kr
DOI 10.1007/s12206-008-0409-6

a channel. They also modeled the effects of humidity at the anode inlet on the performance of the PEFC. Yi and Nguyen [8] developed an advanced model to compare different fuel cell designs with co-flow and counter-flow heat exchangers. Rogg et al. [9] presented the reasons for the cooling limits of fuel cells designed for vehicles. Zhang et al. [10] reported a technique to model the thermal system of a PEFC stack, which estimated the fundamental thermal-physical behaviors of the thermal system. They used a lumped thermal mass model to analyze the system.

The studies on the performance and design of the cooling system are very limited in open literature. Most analyses have been executed by using a two-dimensional method without considering the variation of heat flux. Therefore, it is necessary to optimize and analyze the complicated cooling system of a fuel cell system. In this study, the configurations of the cooling plates for a PEFC stack are designed and the performance of the fluid flow and heat transfer in the PEFC stack is investigated according to the heat flux and operating conditions of the fuel cell stack by using three-dimensional fluid dynamics with commercial software.

2. Numerical modeling

A PEFC consists of an MEA, a gas diffusion layer (GDL) on each side of the MEA, and two graphite bipolar plates, on which the gas flow channels are machined for the distributions of fuel (hydrogen) and oxidant. Hydrogen gas ionizes at the anode, releasing electrons and creating hydrogen ions. At the cathode, oxygen reacts with the electrons from the electrode and the hydrogen ions from the electrolyte. During this process, the electrons flow from the anode towards the cathode through an external electrical circuit. An electrochemical reaction between hydrogen and oxygen through the MEA produces heat. As shown in Fig. 1(a), a fuel cell stack includes serially connected single unit cells to produce the designed power. Therefore, cooling plates are installed in the fuel cell stack in a repetitive sequence to prevent the fuel cells from overheating [1, 11, 12]. As shown in Fig. 1(b), each cooling plate controls the heat from several unit cells [5].

In this study, a single cooling plate, which is shown in Fig. 2, is modeled by using a CFD program because it is installed between the MEA and has a symmetric structure. The heat flux on both sides of

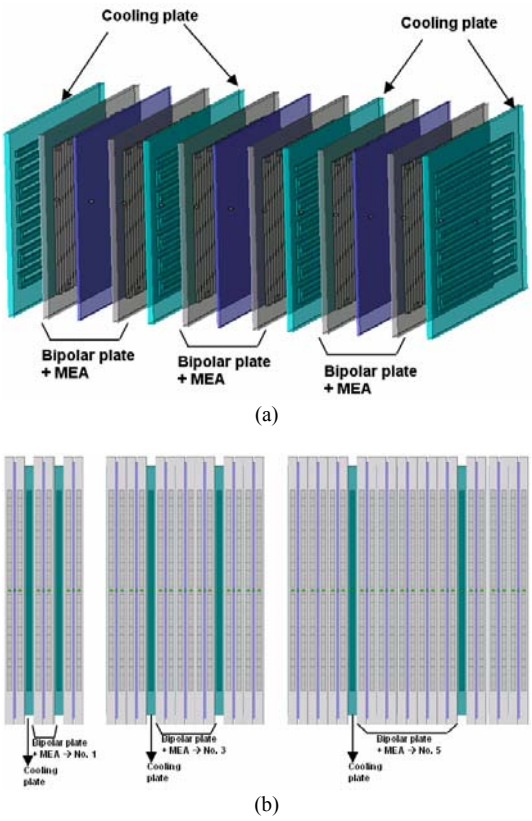

Fig. 1. Schematic of a fuel cell stack.

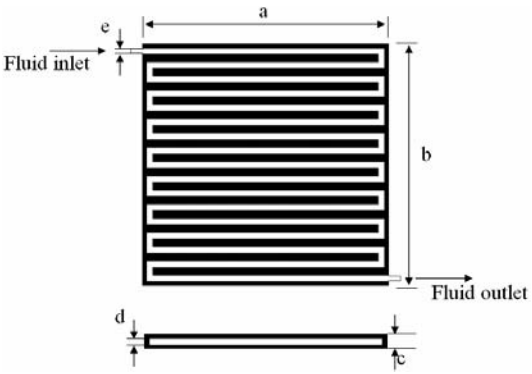

Fig. 2. Structure of a cooling plate.

the cooling plate comes from the heat generated by the electrochemical reaction between the fuel and oxidant in the MEA. For a stack of n cells at current I, the generated heat is determined by using Eq. (1). When all the reaction enthalpy of a hydrogen fuel cell is converted into electrical energy and the water product is in vapor, the output voltage becomes 1.25 V [11].

$$Q = nI(1.25 - V) \tag{1}$$

The cooling plate was made of graphite having a cross sectional area of $0.1\times0.1\text{m}^2$, and the size of a rectangular channel was $0.002\times0.001\text{m}^2$. Table 1 shows the specification and properties of the cooling plate [13]. As shown in Figs. 3(a) and (d), typical serpentine and parallel configurations were applied into the cooling channel to achieve thermal reliability of PEFCs [12, 14]. In addition, Figs. 3(b) and (c) are the modified structures of the typical serpentine type channel (Fig. 3(a)), and Figs. 3(e) and (f) are the modified structures of the typical parallel type channel (Fig. 3(d)) used to improve the thermal reliability of PEFCs.

Table 1. Specifications of the cooling-plate.

Parameter	Condition
Cooling fluid	Water
Inlet temperature of the fluid (K)	313.15
Density of the fluid(kg/m^3)	992.18
Specific heat of the fluid (J/kg·K)	4.1796
Electrical power per fuel cell (W)	29.94
Heat generation per fuel cell (W)	32.44
Heat flux (W/m^2)	1625.0, 4875.0, 8125.0
Inlet hydraulic diameter (m)	0.001
Inlet hydraulic Reynolds number	≤2100
Inlet fluid velocity (m/s)	≤1380

The present simulation was conducted by using the CFD-ACE+, which is a commercial program based on three-dimensional CFD simulation [15]. This program consists of a flow-module and a heat transfer module that solves the flow and temperature fields, respectively. The governing equations include mass, momentum, and energy conservations, which are expressed by Eqs. (2), (3), and (4), respectively. All simulations are conducted by using the segregated method [16].

$$\frac{\partial}{\partial x_i}(\rho u_i) = 0 \tag{2}$$

$$\frac{\partial}{\partial x_i}(\rho u_i u_j) = \frac{\partial}{\partial x_i}\left(\mu\frac{\partial u_j}{\partial x_i}\right) - \frac{\partial p}{\partial x_j} \tag{3}$$

$$\frac{\partial}{\partial x_i}(\rho u_i T) = \frac{\partial}{\partial x_i}\left(\frac{k}{c_p}\frac{\partial u_j}{\partial x_i}\right) \tag{4}$$

The heat flux provided on the left and right surfaces of the single cooling plate was determined by the heat generation as given in Eq. (1). Therefore, the heat flux can be expressed as

$$q'' = \frac{Q}{A} = \frac{nI(1.25 - V)}{A} \tag{5}$$

Water was used as the working fluid. Normal velocity specified as the mean flow velocity at the inlet port was calculated by using the hydraulic diameter

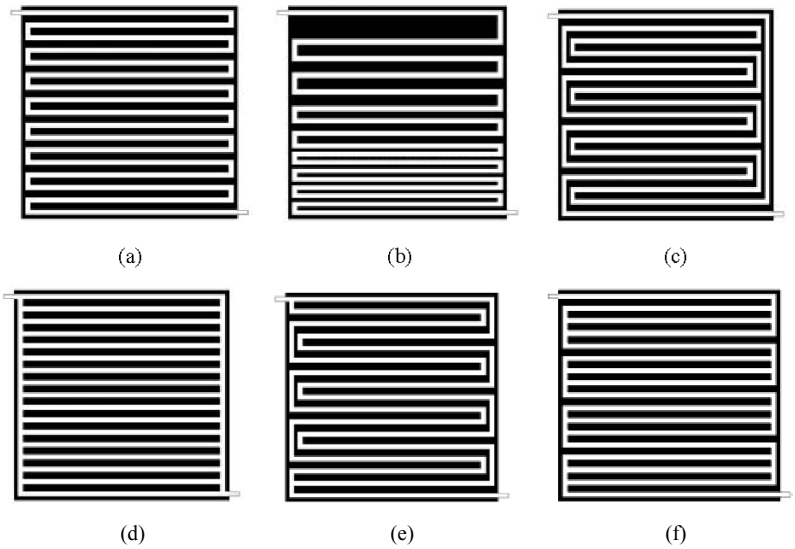

Fig. 3. Configurations of flow channels in the cooling plate.

and hydraulic Reynolds number, which were expressed by Eqs. (6) and (7), respectively. Both of the hydraulic diameter and hydraulic Reynolds number were defined at the inlet port of the cooling plate.

$$D_h = \frac{4A_c}{P} \tag{6}$$

$$\mathrm{Re} = \frac{\rho u D_h}{\mu} \tag{7}$$

No-slip condition on the side walls was applied and the environment of the solid in contact with the surrounding was considered to be perfectly insulated. Outlet pressure was assumed atmospheric pressure. The geometry for the present simulation was based on a fuel cell stack designed for 5kW, in which each cooling plate cools one, three, and five unit cells. The heat fluxes for one, three, and five unit cells are 1625, 4875, and 8125W/m^2, respectively. Simulation conditions are listed in Table 2.

Table 2. Simulation conditions for the cooling-plates.

Parameter	Condition
Cooling fluid	Water
Inlet temperature of the fluid (K)	313.15
Density of the fluid(kg/m^3)	992.18
Specific heat of the fluid (J/kg·K)	4.1796
Electrical power per fuel cell (W)	29.94
Heat generation per fuel cell (W)	32.44
Heat flux (W/m^2)	1625.0, 4875.0, 8125.0
Inlet hydraulic diameter (m)	0.001
Inlet hydraulic Reynolds number	≤2100
Inlet fluid velocity (m/s)	≤1380

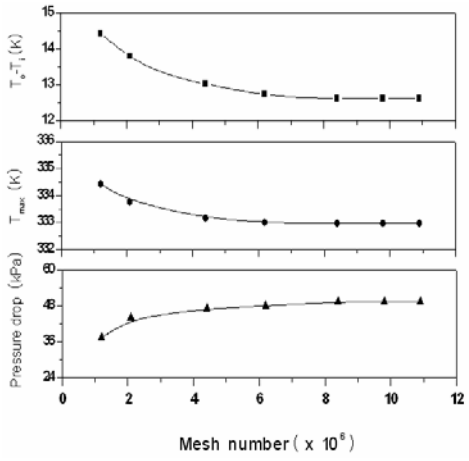

Fig. 4. Grid validation.

3. Results and discussion

The fluid flow and heat transfer characteristics in the cooling plates were simulated by varying the heat flux and the operating conditions of the fuel cell stack. To assure more accurate predictions, convergence and discretization errors were minimized. The convergence error of the iteration scheme was checked by monitoring both the residual factors for the individual conservation equations and field values at a particular point in the flow domain. The discretization error was also minimized by checking the dependence on the grid density. The simulations for Model 1 were conducted by varying a structured grid over 126,000. The temperature difference between the inlet and outlet of the water, the maximum surface temperature over the cooling plate, and the pressure drop through the cooling plate were investigated by varying the grid number. As shown in Fig. 4, these parameters remained nearly constant when the grid number increased beyond 8,000,000. Therefore, further numerical analysis was executed at the grid number of 8,000,000.

3.1 Performance of cooling plates at constant heat flux

The maximum surface temperature is the most important factor in preventing thermal damage of the PEFC. Figs. 5 and 6 show the maximum surface temperature and the temperature difference between the water inlet and outlet as a function of the Reynolds number, respectively, at a constant heat flux. The Reynolds number at the inlet varied from 500 to 2100 at the inlet temperature of 313K. Advanced serpentine type Models 2 and 3 were designed to enhance the cooling performance of the basic serpentine type Model 1. The cooling capacities of the serpentine type models (Models 1, 2, and 3) were very similar because the temperature differences between the inlet and outlet of these models were nearly the same due to their equal flow rate. However, the maximum temperature of Model 3 was less than that of Models 1 and 2 for all Reynolds numbers. The relatively high temperature of the fluid at the outlet of Model 1 was due to the heat absorption through the channel (Fig. 7(a)), which caused a high surface temperature around outlet area. These trends in a typical serpentine cooling plate were also observed by Jeon et al. [17].

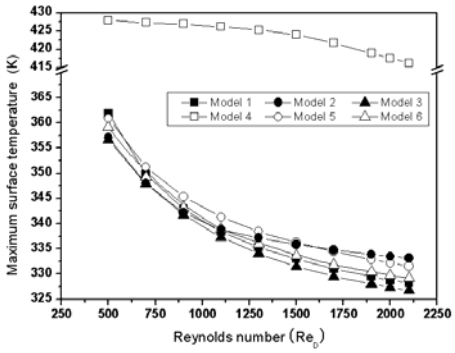

Fig. 5. Variations of the maximum surface temperature according to Reynolds number at the heat flux of 4875.0 W/m^2.

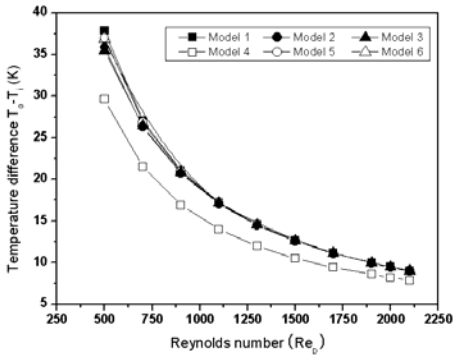

Fig. 6. Temperature difference between the inlet and outlet of the cooling plate according to Reynolds number.

The use of Model 2 reduced the space between the channels as the fluid approached to the outlet. The temperature profile in Model 2 around the outlet area was improved, but the local temperature around the inlet area was increased due to the large spacing between the channels in the inlet region as shown in Fig. 7(b). Model 3 has the same space between the channels as Model 1. However, the cooling fluid flows between inlet and outlet area alternately. Model 3 represented a similar temperature difference between the inlet and outlet of the fluid as those of Models 1 and 2. In addition, Model 3 showed a lower maximum temperature even though it had a higher uniform temperature across the entire area (Fig. 7(c)).

Model 4 has a parallel type fluid flow channel. Model 5 has two parallel type fluid flow channels, which include serpentine type sub-passages. Model 6 has three parallel type flow channels, which also include serpentine type sub-passages. In Model 4, the high temperature region was wide in the central area. The predicted maximum temperature for Model 4 was higher than the limitation of PEFC tolerance (Fig. 7(d)). The numbers of parallel fluid paths in Models 5 and 6 were less than those of Model 4. The maximum temperature and central thermal stratification in Models 5 and 6 were significantly reduced, and the high temperature region was observed around the outlet of

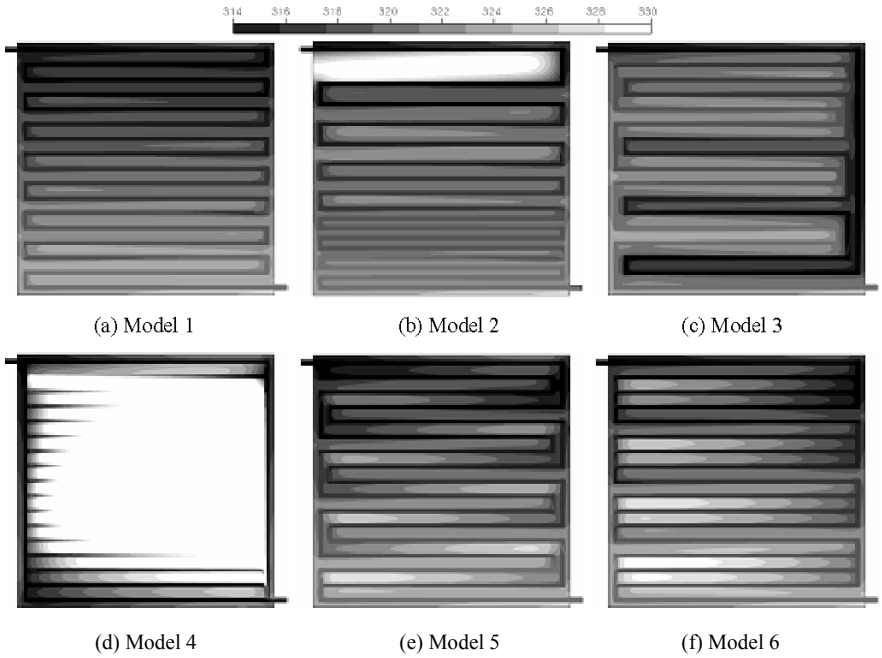

Fig. 7. Temperature distributions in the cooling plates at Re_D=2000 and the heat flux of 4875.0 W/m^2.

the channel, as shown in Figs. 7(e) and (f). Thermal stratifications observed in Models 5 and 6 due to the restrictions of the parallel passages into two or three yielded a more stable distribution of cooling fluid closer to cooling flow in the serpentine type models. The temperature distribution and the maximum surface temperature in Model 6 were very similar to those in Model 5, but Model 6 showed slightly lower maximum surface temperature than did Model 5 at high Reynolds numbers.

In order to assure thermal reliability of the PEFC, it is essential to control the maximum surface temperature below a certain level. Based on the thermal analysis at a constant heat flux, Models 3 and 6, which represented the lowest maximum surface temperature, were selected as the optimum cooling plate configurations among the serpentine type models and the parallel type models, respectively.

3.2 Heat transfer and fluid flow characteristics of optimized cooling plates

Thermal management for the PEFC removes the heat produced by the electrochemical reaction of the energy during high power density operation. In addition, uniform temperature distribution is required under various operating conditions [1, 14]. The performance of Models 3 and 6, which were selected as the optimum models, was analyzed with the variation of heat flux.

Fig. 8 shows the variations of the maximum surface temperatures with respect to heat flux in Models 3 and 6. As the heat flux increased, the maximum temperature of the cooling plates for both models increased due to the fixed heat capacity of the working fluid. The increasing slope of the maximum temperature with respect to the heat flux at high Reynolds number was lower than that at low Reynolds number. However, the maximum surface temperature of Model 3 was lower than that of Model 6 at all conditions. In addition, the increasing slope of the maximum surface temperature with respect to the heat flux for Model 3 was lower than that for Model 6. The PEFC is very sensitive to the high temperature envi-

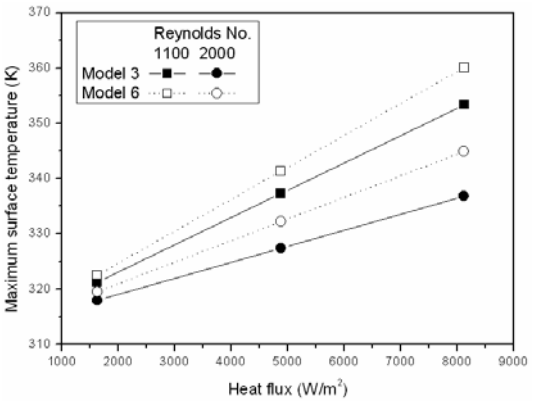

Fig. 8. Variations of the maximum surface temperature according to heat flux.

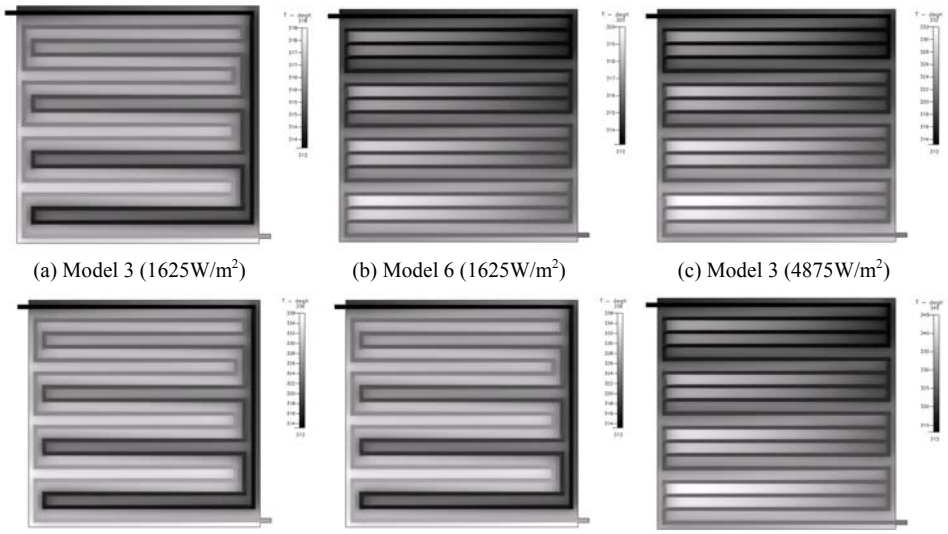

(a) Model 3 (1625W/m^2) (b) Model 6 (1625W/m^2) (c) Model 3 (4875W/m^2)

(d) Model 6 (4875W/m^2) (e) Model 3 (8125W/m^2) (f) Model 6 (8125W/m^2)

Fig. 9. Temperature distributions in Models 3 and 6 according to heat flux at Re_D=2000.

ronment inside a fuel cell because it operates at a relatively lower temperature around 80°C. When the stack temperature increases, the relative humidity of the membrane will decrease, and this decrease deteriorates the ionic conductivity of the membrane. Therefore, humidification devices are required to maintain the ionic conductivity of the membrane. When sufficient humidification is provided for all conditions, the relative humidity will control the stack temperature to a reasonable level. However, since there is a limitation on the amount of humidification, it is very important to keep the operating temperature below a certain level by using stack cooling. In addition, non-uniform temperature distribution reduces the kinetic reaction rate and increases the ohmic losses in the electrolyte.

Fig. 9 shows the temperature profiles of Models 3 and 6 with the variation of heat flux at the Reynolds number of 2000. Model 3 shows higher temperature uniformity than Model 6 at all heat flux conditions. In Model 3, the outlet temperature of the fluid increased with the increase of the heat flux, but the surface temperature distribution near the outlet area of the fluid was similar to that near the inlet area. Model 3 represents a lower maximum temperature and a higher uniformity of the surface temperature across the entire area because of the structure of the fluid path.

In Model 6, the thermal stratification increased with the increase of heat flux as shown in Fig. 9. High temperature was observed near the outlet area of the fluid. The relatively high temperature of the fluid at the outlet area was caused by the heat absorption through the channel. The fluid temperature of the outlet area increased with the increase of heat flux because three parallel flow channels of Model 6 had serpentine type sub-paths. Therefore, the cooling capacity of the fluid around outlet zone was significantly reduced due to the smaller temperature difference between the fluid and the surface with the increase of the heat flux. As a result, the maximum surface temperature and the increasing slopes according to the heat flux for Model 3 were lower than those for Model 6. The maximum surface temperatures of Model 3 were lower by 1.6K and 8.1K than those of Model 6 at heat fluxes of 1625W/m^2 and 8125W/m^2, respectively, at a Reynolds number of 2000.

It is very important to develop technologies for controlling the temperature of the PEFC. However, the maximum surface temperature is difficult to sense because the PEFC consists of several unit cells with cooling plates. Fig. 10 shows the maximum surface temperature as a function of the outlet temperature of the fluid. The outlet temperature was linearly proportional to the maximum outlet temperature at all conditions. Therefore, the outlet temperature of the fluid can be used as a control parameter to achieve thermal reliability of the PEFC.

The pressure drop through the cooling plates should be minimized to reduce pumping power. Fig. 11 shows the pressure drop through the cooling plate as a function of the inlet Reynolds number. The pressure drop for Model 3 was much higher than that for Model 6. Fig. 12 represents the velocity distributions in Model 3 at Reynolds numbers of 500 and 2000. Significant velocity distortion was observed as the flow passed through the bend and large recirculation was also observed downstream of the bend. Acceleration occurred along the region near the outer wall, while deceleration along the inner wall at the bend. These changes led to flow separation and the formation of recirculation near the outer wall in the initial part of the bend and near the wall in the latter half of the bend. Therefore, the pressure drop around the bend was much higher than that in the straight region. The size and intensity of both vortices at the inner corner and outer corner increased with the increase of the Reynolds number. The distance between successive bends in a serpentine channel is another dominant parameter affecting the flow. The close presence of an upstream bend suppresses the flow separation to some extent at the second bend. This beneficial effect is reduced as the bend separation distance increases, as shown in Fig. 12(c) and (d). Therefore, it is very important to consider the bend arrangement in the serpentine flow path to reduce the pressure drop.

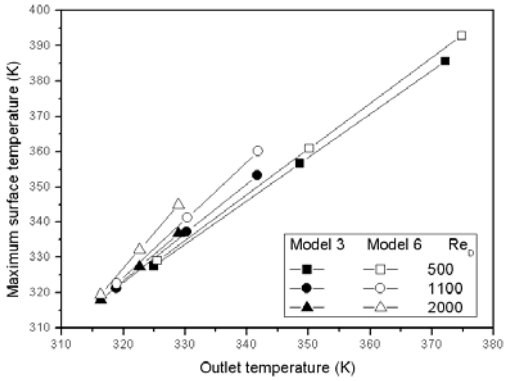

Fig. 10. Variations of the maximum surface temperature according to outlet temperature.

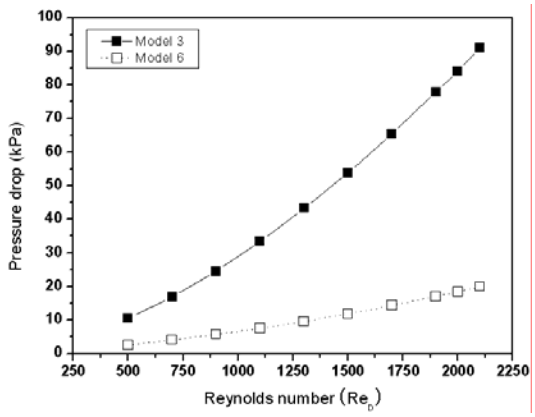

Fig. 11. Pressure drop through the cooling plate as a function of Reynolds number.

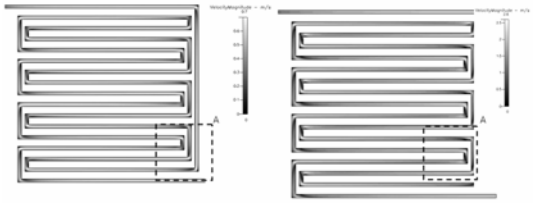

(a) Velocity profile (Re_D=500) (b) Velocity profile (Re_D =2000)

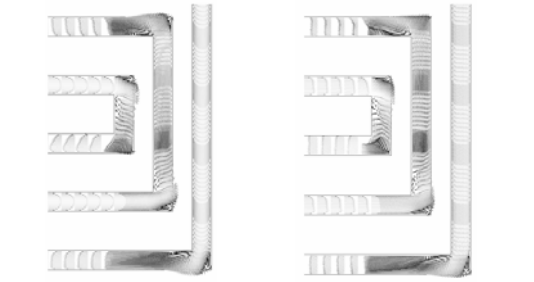

(c)Velocity at zone A (Re_D=500) (d) Velocity at zone A (Re_D =2000)

Fig. 12. Velocity profile of Model 3.

The number of bends for Model 6 was less than that for Model 3. Therefore, the flow recirculation or distortion of the former was much less than that for the latter, as shown in Fig. 13. In addition, the flow velocity through the parallel channels was lower than that through the single channel. The increasing rate of flow velocity with the increase of Reynolds number for Model 6 was less than that for Model 3. For these reasons, the pressure drop and the slope according to Reynolds number for Model 6 were much lower than those for Model 3. Therefore, to reduce the pressure drop, it is necessary to control the equilibrium length of the cooling paths while keeping a higher uniform temperature across the entire plate.

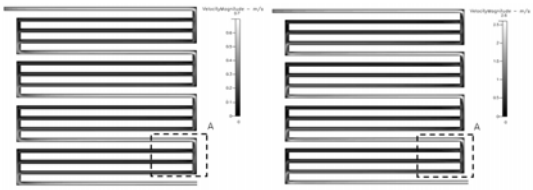

(a) Velocity profile (Re_D=500) (b) Velocity profile (Re_D =2000)

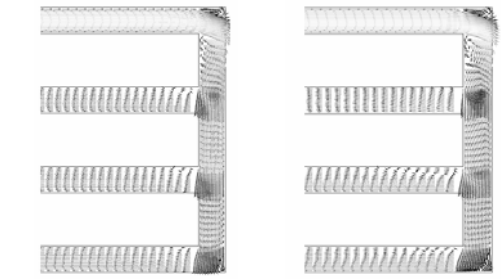

(c) Velocity at zone A (Re_D =500) (d) Velocity at zone A (Re_D =2000)

Fig. 13. Velocity profile of Model 6.

4. Conclusions

In this study, the cooling performance of the cooling plates for the PEFC was analyzed by using three-dimensional computational fluid dynamics. In Model 1, having a typical serpentine flow path, the relatively high temperature of the fluid around the outlet of fluid was caused by the heat absorption through the channel, which led to the high surface temperature. Model 3, which was designed to improve the cooling performance of other serpentine models including Models 1 and 2, showed lower maximum surface temperature among the serpentine models even though it showed higher uniform temperature across the entire area because its cool and warm paths were located alternately. Model 6, which was designed to improve non uniform distribution of fluid flow in a typical parallel cooling plate of Model 4, showed higher cooling performance than other parallel type models including Models 4 and 5. The maximum surface temperature of Models 3 and 6, which had the best performance among the serpentine and parallel type models, respectively, increased with the increase of heat flux. However, Model 3 showed higher cooling performance than Model 6. Model 3 showed lower maximum surface temperature and higher uniformity of surface temperature than Model 6. The thermal performance improvement of Model 3 over Model 6 increased with the increase of the heat flux. However, the pressure drop of Model 3 was higher than that of Model 6 because Model 3 had relatively high flow

velocity through the channel and more number of bends than Model 6.

Acknowledgments

This work was sponsored by the Basic Research Program of the Korea Science & Engineering Foundation (Grant no. R01-2006-000-11014-0).

Nomenclature

A : Area (m^2)
A_c : Cross-sectional area of channel (m^2)
c_p : Specific heat at constant pressure (kJ kg^{-1} K^{-1})
D_h : Hydraulic diameter (m)
i, j : Index of tensor notation
I : Current (A)
n : Number of unit cell
p : Pressure (Pa)
P : Wetted perimeter of channel (m)
Q : Heat generation (W)
q'' : Heat flux (W m^{-2})
Re_D : Hydraulic Reynolds number
T : Temperature (K)
T_i : Inlet temperature (K)
$T_{\max}$: Maximum surface temperature (K)
T_o : Outlet temperature (K)
u : Flow velocity (m s^{-1})
V : Voltage (V)

Greek symbols

ρ : Density (kg m^{-3})
k : Thermal conductivity (W m^{-1} K^{-1})
μ : Dynamic viscosity (kg m^{-1} s^{-1})

References

[1] N. Djilali and D. Lu, Influence of heat transfer on gas and water transport in fuel cells, *International Journal of Thermal Science,* 41 (1) (2002) 29-40.

[2] P. F. Oosterkamp, Critical issues in heat transfer for fuel cell systems, *Energy Conversion & Management,* 47 (20) (2006) 3552-3561.

[3] J. V. C. Vargas, J. C. Ordonez and A. Bejan, Fuel cells constructal optimization and research perspective, Fuel Cell Science, Engineering and Technology, Rochester, New York, USA, 2004, 67-78.

[4] J. M. Ogden, M. M. Steinnbugler and T. G. Kreutz, A comparison of hydrogen, methanol and gasoline as fuels for fuel cell vehicles: Implications for vehicle design and infrastructure development, *Journal of Power Sources,* 79 (2) (1999) 143-168.

[5] F. Barbir, PEM Fuel Cells: Theory and Practice, Elsevier Academic Press, Burlington, 2005, pp. 76-81.

[6] G. Inoue, T. Yoshimoto, Y. Matsukuma, M. Minemoto, H. Itoh and S. Tsurumaki, Numerical analysis of relative humidity distribution in polymer electrolyte fuel cell stack including cooling water, *Journal of Power Source,* 162 (1) (2006) 81-93.

[7] T. Nguyen and R. White, A water and heat management model for proton-exchange-membrane fuel cells, *Journal of Electrochemical Society,* 140 (8) (1993) 2178-2186.

[8] J. Yi and T. Nguyen, An along-the channel model for proton exchange membrane fuel cells, *Journal of Electrochemical Society,* 145 (4) (1998) 1149-1159.

[9] S. Rogg, M. Hoglinger, E. Zwittig, C. Pfender, W. Kaiser and T. Heckenberger, Cooling modules for vehicles with a fuel cell drive, *Fuel Cells,* 3 (3) (2003) 153-158.

[10] Y. Zhang, M. O. Q. Lu, J. Luo and X. Li, A model predicting performance of proton exchange membrane fuel cell stack thermal systems, *Applied Thermal Engineering,* 24 (4) (2004) 501-513.

[11] J. Larminie and A. Dicks, Fuel Cell System Explained, 2nd Ed., Wiley, 2002.

[12] X. Li, Principles of Fuel Cells, Taylor & Francis Group, 2006.

[13] H. O. Pierson, Handbook of Carbon, Graphite, Diamond and Fullerenes: Properties, Processing and Applications, Noyes Publications, 1993.

[14] F. C. Chen, Z. Gao, R.O. Loutfy and M. Hecht, Analysis of optimal heat transfer in a PEM fuel cell cooling plate, *Fuel Cells,* 3 (4) (2003) 181-188.

[15] ESI US R&D, CFD-ACE+ Theory Manual, ESI US R&D Inc., 2004.

[16] S. V. Patankar, Numerical Heat Transfer and Fluid Flow, Hemisphere, Washington DC, 1980.

[17] J. W. Jeon, Y. Kim, J. M. Choi, H. Kang and D. W. Cheon, Performance comparison of liquid-cooling with air-cooling heat exchangers for telecommunication equipment, The 3rd Asian Conference on Refrigeration and Air-conditioning, Korea, 2006.